Research Square

Preprints are preliminary reports that have not undergone peer review.
They should not be considered conclusive, used to inform clinical practice,
or referenced by the media as validated information.

Engineering of a plant ribosylated nucleotide immune second messenger

Steven Cheng

scheng@mpipz.mpg.de

Max Planck Institute of Plant Breeding Research (MPIPZ)

Julian Strippel

Department of Chemistry and Biochemistry, Institute of Organic Chemistry, University of Cologne

Federica Locci

MPIPZ

Alexander Mandel

MPIPZ https://orcid.org/0009-0008-4644-085X

Maria Chalikiopoulou

MPIPZ

Christof Domnick

Department of Chemistry and Biochemistry, Institute of Organic Chemistry, University of Cologne
https://orcid.org/0000-0002-9049-5304

Katharina Klupsch

Department of Chemistry and Biochemistry, Institute of Organic Chemistry, University of Cologne
https://orcid.org/0000-0002-5713-4718

Tak Lee

MPIPZ https://orcid.org/0000-0001-7008-7605

Mai Trinh Nguyen

MPIPZ

Silvina Perin

MPIPZ

Sarwar Aziz

Department of Chemistry and Biochemistry, Institute of Organic Chemistry, University of Cologne

Jaqueline Bautor

MPIPZ

Stephanie Kath-Schorr

Department of Chemistry and Biochemistry, Institute of Organic Chemistry, University of Cologne

Jane Parker

MPIPZ https://orcid.org/0000-0002-4700-6480

Article

Keywords:

Posted Date: September 22nd, 2026

DOI: https://doi.org/10.21203/rs.3.rs-10080789/v1

License: This work is licensed under a Creative Commons Attribution 4.0 International License.
Read Full License

Additional Declarations: Yes there is potential Competing Interest. A patent application for the preparation of pRib-AMP and related derivatives has been filed (EP25191966.8). SCLH and JS are involved in pre-commercial innovation activities with Max Planck Innovation through the Max!mize program based on the patent and the findings presented in the manuscript.

Abstract

Diseases cause major losses in crop production globally. Deployment of conventional pesticides targeting microbes and pests is increasingly restricted due to environmental damage. We have developed a high-yielding chemical route to synthesize a plant immune second messenger, phospho-ribosyl-adenosine monophosphate (pRib-AMP) and engineered pRib-AMP derivatives. Using knowledge of the pRib-AMP molecular mode of action in promoting plant transcriptional defence, we performed structure-based engineering of a stabilized bioactive pRib-AMP derivative (Thio-pRib-AMP). When exogenously applied to *Arabidopsis* plants, pRib-AMP, and Thio-pRib-AMP with higher potency, stimulated immunity via the pRib-AMP authentic receptor and defence execution machinery, leading to reduced pathogen infection. Dose-response and transcriptome assays revealed a need to tune Thio-pRib-AMP applications for enhanced disease resistance without incurring a growth penalty in *Arabidopsis*, *Nicotiana benthamiana* and oilseed rape. This study describes a biotechnology framework for harnessing the properties of natural plant immune stimulants to generate protective agents for a broad range of crops.

Main

Crop productivity is severely limited by pathogens and pests. Of the crop protection strategies developed in agriculture, utilization of chemical pesticides has dominated. Often pesticide treatments are not specific to a pest or microbe and thus can also target beneficial organisms, leading to detrimental impacts on the environment and human health[1–3]. A further danger of widespread chemical pesticide use is the occurrence of pathogen and pest resistance[4]. These negative outcomes have prompted global efforts to phase out hazardous pesticides. The shrinking repertoire of deployable agents creates a need for alternative, environmentally safe crop protection strategies[5,6].

Angiosperm plants (dicots and monocots), comprising the major food crops, possess an innate immune system which deploys cell-surface (receptor-like kinase (RLK) or receptor-like protein (RLP)) and intracellular (nucleotide-binding/leucine rich repeat (NLR)) receptors to detect pathogen disturbance and trigger resistance. Considerable advances have been made in understanding the evolutionary dynamics of plant hosts with disease-causing pathogen strains and the biochemical processes underpinning immune receptor activation and signalling [7–10], creating opportunities to engineer immune receptors for sustained disease resistance in transgenic crops [11,12].

Here we explore a different biotechnology strategy to enhance crop disease resistance which capitalizes on recently discovered ribosylated nucleotide immune second messengers (SMs) in angiosperm plants[10]. The SMs 2'-(5"-phosphoribosyl)-5'-adenosine monophosphate (pRib-AMP) and its diphosphate form (pRib-ADP) are produced by Toll-Interleukin-1 Receptor (TIR) enzyme hydrolysis of NAD^+ [13,14]. Pathogen-induced TIR-domain NLRs (TNLs) and TIR-only proteins signal as NADase enzymes[15–20]. Of TIR/TNL generated cyclic and non-cyclic nucleotides, non-cyclic pRib-AMP/ADP activate an angiosperm

immune regulatory module connecting cell-surface and intracellular receptors to transcriptional defence that limits pathogen growth[18,21–24]. The module consists of Enhanced Disease Resistance 1 (EDS1) in a dimer with Phytoalexin Deficient 4 (PAD4) which, upon SM binding, conformationally activates a sub-family of variant coiled-coil domain signalling NLRs (RNLs) called Activated Disease Resistance1 (ADR1) to confer immunity[13,24]. Genes for this TIR enzyme-activated EDS1-PAD4-ADR1 module are conserved across dicot and monocot genomes[25,26]. Moreover, the dicot model *Arabidopsis thaliana* (*Arabidopsis*) and monocot rice (*Oryza sativa*) employ the same TIR-EDS1-PAD4-ADR1 biochemical mode of action to restrict infection by a broad range of pathogens[13,18,24]. A second dicot-specific module consisting of EDS1 in a dimer with Senescence Associated Gene101 (SAG101) and co-functioning N requirement gene1 (NRG1)-family RNLs is stimulated by different TIR/TNL catalyzed non-cyclic SMs, ADPr-ATP and di-ADPR[14] to promote host immune-related cell death [27,28,29] .

We explored whether pRib-AMP or its chemical derivatives could be deployed as immune stimulants in angiosperm plants. We describe a new high-yielding chemical synthetic route for pRib-AMP and a versatile platform to engineer pRib-AMP modified forms. We establish that pRib-AMP and an engineered derivative, Thio-pRib-AMP, promote transcriptional defence and pathogen resistance specifically via the EDS1-PAD4-ADR1 node when applied to *Arabidopsis* intact cells and plants. Thio-pRib-AMP exhibits ~ 100-fold higher potency than pRib-AMP for transcriptional reprogramming, consistent with its increased hydrolytic stability and sustained action at nanomolar doses in *Arabidopsis*. We further establish that Thio-pRib-AMP sprayed or infiltrated on leaves increases pathogen resistance in a solanaceous plant model *Nicotiana benthamiana* and a commercial winter *Brassica napus* (rapeseed oil) variety, Vamos. These findings highlight a new path towards broad-action immune stimulants for crops.

Results

Chemical synthesis of pRib-AMP and derivatives

Previously, chemical synthesis of pRib-AMP was achieved by a 15-step procedure[13]. We developed a simpler method to produce pRib-AMP over 5 linear steps with a total yield of 42% (Fig. 1a). Our design principle was to generate pRib-AMP and pRib-AMP derivatives from a common synthetic precursor, Rib-A, through a 5´-regioselective functionalisation (Fig. 1a)[30]. Starting from N^6-benzoylated adenosine, we protected the 3´- and 5´-hydroxy groups with a bridged silyl protecting group (di-*tert*-butylsilyl, DTBS) (Fig. 1a; step i). We next employed this protected nucleoside (Fig. 1a; step ii) in a β-selective ribosylation reaction using 1-O-Acetyl-2,3,5-tri-O-benzoyl-β-D-ribofuranose as the ribosyl-donor in the presence of $SnCl_4$ as a Lewis acid[31]. This step exclusively gave the β-anomer (Fig. 1a; step iii), validated by crystal structure analysis (Supplementary Information). Stepwise deprotection of the silyl groups by tetrabutylammonium fluoride (TBAF) (Fig. 1a; step iv), and the benzoyl groups by ammonia (Fig. 1a; step v), produced Rib-Adenosine (Rib-A) in a 4-step procedure with 50% overall yield. A final phosphorylation step was accomplished using proton sponge as a sterically demanding base together with $POCl_3$ as phosphorylating agent. Triethylammonium (TEA) was used as counterion to obtain TEA_4pRib-AMP from

Rib-A with a yield of 83% (Fig. 1a). Synthesis of pRib-AMP provided pure compound to test pRib-AMP in vivo bioactivity.

Exogenously applied pRib-AMP promotes EDS1-PAD4-ADR1 dependent immunity in Arabidopsis

In solution, pRib-AMP is highly polar and negatively charged, which we anticipated would not pass unaided across the cell membrane into the cytoplasm. We therefore applied TEA_4pRib-AMP to a final concentration of 20 µM or 80 µM TEA only (as negative control), with and without the transfection agent lipofectamine 3000 (L3000), to *Arabidopsis* Col-0 (WT) protoplast suspensions[32] (EDF. 1a). Induced expression of *EDS1-PAD4* dependent defence marker genes *CYP71A13*, *CBP60g* and *SARD1* was measured by qRT-PCR (EDF. 1b, Supplementary Table 1). TEA_4pRib-AMP treatment led to defence gene upregulation in the presence and absence of L3000 (EDF. 1b). This suggests that pRib-AMP alone can cross the plant cell membrane for immune transcriptional reprogramming in *Arabidopsis*.

We next investigated whether pRib-AMP stimulates transcriptional defence when infiltrated into *Arabidopsis* seedlings (Fig. 1b). WT treated with TEA_4pRib-AMP, but not its immediate non-phosphorylated precursor Ribose-Adenosine (Rib-A) or TEA only, displayed elevated defence marker gene expression (EDF. 1c), indicating bioactivity of pRib-AMP on seedlings. Transcriptional reprogramming induced by pRib-AMP was lost in *eds1* and *pad4* but maintained in a *sag101* mutant defective in the EDS1-SAG101-NRG1 cell death module[14,27] (Fig. 1c), indicating in vivo signalling specificity of the synthetic pRib-AMP through EDS1-PAD4. We next tested seedling responses of previously characterized *pad4/sag101* (*ps)* double mutant lines complemented with WT PAD4 (*gPAD4^{WT}/ps*) or a PAD4 pRib-AMP binding mutant (*gPAD4^{R314A}/ps)*, and *pad4 sag101* complemented with WT SAG101 (*SAG101^{WT}/ps)*[23]. Only WT and *gPAD4^{WT}/ps* seedlings displayed elevated immune marker gene expression following pRib-AMP treatment (Fig. 1d). Also, pRib-AMP treatment of mutants lacking helper NLRs ADR1/ADR1-L1/ADR1-L2 (*adr1 triple*)[33,34] or NRG1a/NRG1b (*nrg1a/b*)[35] showed that only *adr1 triple* mutant seedlings failed to respond to pRib-AMP (Fig. 1e). These data underscore specificity in synthetic pRib-AMP promotion of immune marker genes through the EDS1-PAD4-ADR1 module.

We considered that induction of *Arabidopsis* defence genes by applied synthetic pRib-AMP might be due to cell-surface receptor recognition of pRib-AMP as a misplaced ligand rather than by pRib-AMP uptake into cells. We therefore applied pRib-AMP to mutants in key cell-surface receptor/co-receptor or signalling components (Supplementary table 3) and measured immune marker gene expression (EDF. 2a). All mutant lines reacted similarly to WT in response to TEA_4pRib-AMP (EDF. 2a). Furthermore, applications of 1 µM to 100 µM TEA_4pRib-AMP to WT plants failed to elicit a reactive oxygen species (ROS) burst, which is a hallmark of canonical cell-surface receptor activation, as detected after pathogen elicitor nlp20 treatment[21] (EDF. 2b). Next, we tested whether TEA_4pRib-AMP application to leaves of mature *Arabidopsis* plants stimulates resistance to virulent *Pseudomonas syringae* pv. *tomato* (*Pst*) strain DC3000 bacteria. WT, *eds1*, *pad4* and *sag101* were pretreated with TEA or TEA_4pRib-AMP. After 1d, the

same leaves were inoculated with *Pst* DC3000 and bacterial numbers measured at 3 dpi (Fig. 1f). Pre-treatment with TEA_4pRib-AMP, but not TEA, reduced bacterial growth in WT by 15-fold (Fig. 1g). A similar reduction in bacteria following TEA_4pRib-AMP application was observed in *sag101* but not in *eds1* or *pad4* plants (Fig. 1g). Therefore, synthetic pRib-AMP treatment promotes bacterial pathogen resistance by stimulation of the EDS1-PAD4-ADR1 signalling node and independently of major cell-surface immunity components.

Chemical derivatization and functional analysis of Thio-pRib-AMP

The new chemical synthetic route was designed to enable late-stage generation of pRib-AMP derivatives from Rib-A as a common synthetic precursor (Fig. 1a and Fig. 2a). We hypothesized that a prodrug ethyl-ester derivative, mono-Et-pRib-AMP (full chemical name provided in Supplementary Information) (Fig. 2a) might mimic the chemical nature of 2´cADPR, a proposed stable storage form and pRib-AMP precursor[18], by reducing the charge at phosphate groups, thereby enhancing membrane permeability. Mono-Et-pRib-AMP was obtained from Rib-A employing ethyl phosphorodichloridate ($POCl_2OEt$) as phosphorylating agent. In parallel, we aimed to assess whether replacement of the two pRib-AMP phosphate groups with a thiophosphate (Fig. 2a)[36,37], might overcome the predicted hydrolytic instability of the phosphoester bonds within pRib-AMP[13]. By employing $PSCl_3$ in the general procedure established for the functionalisation of Rib-A (Fig. 1) we obtained Thio-pRib-AMP (Fig. 2a) with 24% yield (Supplementary Information). We performed ligand docking modelling of pRib-AMP, mono-Et-pRib-AMP and Thio-pRib-AMP into the protein structure of pRib-ADP bound *Arabidopsis* EDS1-PAD4[13,18] (PDB:7XEY) and calculated in silico binding energies (MM/GBSA, molecular mechanics/generalized Born surface area) together with root mean square deviations (RMSD) for each compound (Fig. 2a). The molecular docking results showed that mono-Et-pRib-AMP binds to EDS1-PAD4 poorly. By contrast, Thio-pRib-AMP displayed marginally weaker binding energy and a comparable RMSD to that of pRib-AMP (Fig. 2a).

We infiltrated *Arabidopsis* WT and *pad4* seedlings with 20 µM TEA_2mono-Et-pRib-AMP, TEA_4pRib-AMP or TEA_4Thio-pRib-AMP and measured *CBP60g* and *SARD1* expression at 12 hpi. TEA_2mono-Et-pRib-AMP treatment had a negligible effect on defence marker gene expression compared to TEA_4pRib-AMP (Fig. 2b). By contrast, TEA_4Thio-pRib-AMP elicited stronger *PAD4*-dependent defence marker gene induction than pRib-AMP (Fig. 2b). The low bioactivity of mono-Et-pRib-AMP is consistent with its predicted weak EDS1-PAD4 binding energy (Fig. 2a). The enhanced activity of Thio-pRib-AMP compared to pRib-AMP is not reflected in higher predicted binding energy (Fig. 2a), suggesting that increased potency might be due to greater Thio-pRib-AMP uptake or chemical stability. We measured the depletion of pRib-AMP and Thio-pRib-AMP in *Arabidopsis* lysates over 24 h by LC-mass spectrometry analysis (EDF. 3a). Whereas pRib-AMP displayed a half-life of 1.02 h, consistent with a previous study[13], Thio-pRib-AMP decay was not observed over this time frame (EDF. 3b). Also, we compared pRib-AMP and Thio-pRib-AMP binding to EDS1-PAD4 dimer purified from insect cells by a thermal shift assay (EDF.

4)[13,38]. Both pRib-AMP and Thio-pRib-AMP increased the melting temperature (T_m) of apo-EDS1-PAD4, indicating that both molecules bind to EDS1-PAD4.

We found that a 250 nM Thio-pRib-AMP application to seedlings had similar efficacy as 20 µM pRib-AMP in PAD4-dependent defence gene induction, suggesting ~ 100-fold higher Thio-pRib-AMP bioactivity (Fig. 2c). Furthermore, Thio-pRib-AMP produced more sustained *EDS1-PAD4*-dependent defence gene induction in seedlings compared to pRib-AMP at 6 and 12 hpi (EDF. 3c). Collectively, these results suggest that Thio-pRib-AMP in vivo stability might enable immune stimulation via the EDS1-PAD4-ADR1 node at lower doses than pRib-AMP.

Transcriptional landscape of Arabidopsis WT and pad4 responses to Thio-pRib-AMP

To measure transcriptome changes following TEA_4Thio-pRib-AMP treatment, RNA samples from seedlings infiltrated with 100 nM TEA_4Thio-pRib-AMP for 6 h (Fig. 1b) were prepared for RNA sequencing (RNA-seq). Analysis of differentially expressed genes (DEG) in WT and *pad4* relative to their respective mock treatments revealed seven clusters as shown in a heatmap, with clusters 4 and 5 being enriched in *PAD4* dependent DEG (Fig. 3a, Supplementary Table 2). As displayed in Venn diagrams, 1533 up-regulated and 1357 down-regulated DEG in response to Thio-pRib-AMP were specific to WT (Fig. 3b,c). Gene ontology (GO) analysis showed WT up-regulated DEG (mainly populating clusters 4 and 5) to be enriched in GO terms relating to immune responses (Fig. 3d), whereas down-regulated DEG GO terms mainly related to RNA modification and metabolism (EDF. 5a). We compared the expression profile of Thio-pRib-AMP responsive WT genes with *Arabidopsis* TNL (RRS1-RPS4) receptor triggered *EDS1*-dependent up-regulated DEG in response to *Pst* AvrRps4 bacteria at 8 h[39]. This revealed a significant overlap between treatments and a trend towards higher expression of immune components (for example, *FMO1* and *ALD1* promoters of systemic resistance[40]) in the TEA_4Thio-pRib-AMP treated samples (EDF. 6). Different classes of cell membrane immune receptors and signalling components were also highly represented (EDF. 6), consistent with mutual potentiation between Thio-pRib-AMP and EDS1-PAD4-ADR1 dependent cell-surface receptor signalling[21,22,41]. This analysis shows that exogenously applied Thio-pRib-AMP transcriptionally promotes a broad suite of immune-related defences via EDS1-PAD4.

While there was also a substantial overlap between WT and *pad4* up- (836) and down- (1442) DEG in response to Thio-pRib-AMP these were not related to immune defence. We further noted that 532 up- and 778 down-DEG were specific to the *pad4* mutant response to Thio-pRib-AMP (Fig. 3a-c). GO term analysis revealed that *pad4*-specific up-regulated DEG were mainly associated with membrane raft localization, responses to light signalling and metabolic processes (EDF. 5b). The *pad4* down-regulated DEG were enriched in protein folding, oxidative and other stress responses (EDF. 5c). These data suggest that functional EDS1-PAD4 signalling dampens Thio-pRib-AMP induced gene expression reprogramming, perhaps to maintain cell and tissue homeostasis. Alternatively, Thio-pRib-AMP has one or more immune non-related targets.

Thio-pRib-AMP spray treatment bolsters disease resistance in Arabidopsis and N. benthamiana

Induced plant defence leading to pathogen resistance can be associated with a growth trade-off. We therefore determined the minimal Thio-pRib-AMP effective dose for pathogen resistance without negatively impacting plant growth. Leaves of mature *Arabidopsis* WT and *pad4* plants were sprayed with TEA or 50 nM and 100 nM TEA_4Thio-pRib-AMP (EDF. 7a). At 8 d post treatment, plant fresh weight measurements showed that 100 nM Thio-pRib-AMP led to growth reduction in WT but not *pad4* plants, whereas 50 nM TEA_4Thio-pRib-AMP did not affect plant growth (Fig. 4a,b). Next, we compared 50 nM and 100 nM TEA_4Thio-pRib-AMP spray pre-treatments in limiting *Pst* DC3000 infiltrated 1 d later into WT and *pad4* leaves (EDF. 7b). The 50 nM and 100 nM TEA_4Thio-pRib-AMP reduced bacterial numbers and disease symptoms compared with TEA treatment, whereas bacteria were not reduced in *pad4* leaves (Fig. 4c, d). These findings suggest that a disease resistance benefit of Thio-pRib-AMP can be attained at a low dose without impairing plant growth.

Notably, Thio-pRib-AMP spray treatment of *Arabidopsis* also increased resistance to a virulent strain (Noco2) of the biotrophic oomycete pathogen, *Hyaloperonospora arabidopsidis* (*Hpa*) which causes downy mildew disease. WT and *pad4* plants were sprayed with TEA, 50 or 100 nM TEA_4Thio-pRib-AMP and inoculated 1 d after by spraying *Hpa* Noco2 onto leaves (EDF. 7c). *Hpa* Noco2 conidiospore production was strongly reduced on WT but not *pad4* leaves pretreated with both 50 and 100 nM TEA_4Thio-pRib-AMP, compared to TEA-treated plants (Fig. 4e). The genetically resistant *Arabidopsis* Ws-2 accession displayed full resistance to Noco2 (Fig. 4e). We used trypan-blue staining of leaves to detect *Hpa* infection structures and host cell death microscopically[42]. This revealed that WT treated with 50 nM TEA_4Thio-pRib-AMP slowed *Hpa* Noco2 hyphal growth and conidiophore formation without triggering cell death observed in Ws-2 (Fig. 4f). The *pad4* mutant, by contrast, was heavily colonized by *Hpa* in TEA- and TEA_4Thio-pRib-AMP treated plants (Fig. 4f). We concluded that 50 nM TEA_4Thio-pRib-AMP spray treatment of *Arabidopsis* reduces bacterial and oomycete infection via EDS1-PAD4 defence stimulation.

N. benthamiana (*Nb*) is an infection model for solanaceous crops (such as tomato, potato and pepper) and predominantly uses TIR- and TNL-catalysed ADPr-ATP and di-ADPR SMs activating the EDS1-SAG101-NRG1 module to confer pathogen resistance and host cell death[35,43,44]. *Nb* EDS1-PAD4-ADR1 has a role in stomatal immunity[45]. We tested whether TEA_4Thio-pRib-AMP treatment enhances *EDS1-PAD4* dependent pathogen resistance in *Nb* by infiltrating TEA or 500 nM TEA_4Thio-pRib-AMP into leaves of WT, *Nb pad4* and *Nb sag101a sag101b* plants and spray inoculating 1 d later with virulent *Pst* strain DC3000 ΔHopQ1-1[45] (Fig. 5a). WT and *Nb sag101ab* reduced bacterial numbers by 10-15-fold at 6 dpi in TEA_4Thio-pRib-AMP compared to TEA treated plants, whereas bacterial numbers in *pad4* plants did not differ between treatments (Fig. 5b). The 500 nM TEA_4Thio-pRib-AMP treatment also alleviated macroscopic bacterial disease symptoms in WT and *sag101* but not *pad4* plants (Fig. 5c). These results show that the *Nb* EDS1-PAD4-ADR1 node limits *Pst* bacterial infection after applying Thio-pRib-AMP to leaves.

Thio-pRib-AMP protects rapeseed oil crop plants from disease

We tested Thio-pRib-AMP efficacy in the German rapeseed (*Brassica napus; Bn*) commercial cultivar Vamos by spraying leaves with TEA or 100 nM and 250nM TEA_4Thio-pRib-AMP and measuring induced expression of defence-related genes *BnCBP60g* and *BnEDS1*. Thio-pRib-AMP spray at 100 nM was sufficient to transcriptionally induce *BnCBP60g* and *BnEDS1* (Fig. 5d) and reduce *Pst* DC3000 infection in leaves (Fig. 5e, f).

Discussion

In this study, we provide a new chemical engineering strategy and initial proof-of-concept for SM delivery and immune bioactivity in plants. Our results highlight the potential benefit, and challenges, of pursuing nucleotide-based immune stimulants as crop protectants against disease.

One major biotechnological challenge is to generate useful compounds simply and cheaply. Our designed high-yielding synthesis route to Rib-A as precursor of pRib-AMP, Thio-pRib-AMP and further derivatives (Fig. 1a, 2a) creates a basis to scale-up chemical synthesis for wider application. Another anticipated hurdle was effective delivery of polar pRib-AMP and Thio-pRib-AMP molecules to the receptor machineries inside cells. *Arabidopsis* protoplast (EDF. 1a, b), whole seedling and mature plant responses to exogenous pRib-AMP and Thio-pRib-AMP (Fig. 1c, e, Fig. 2b, c, Fig. 3), suggest that both compounds are able to cross the cell wall and cell membrane to stimulate EDS1-PAD4-ADR1 mediated transcriptional defence and pathogen resistance (Fig. 1g, Fig. 4). In future studies, the bioactive molecules might be directly monitored in plant cells and tissues using, for example, engineered trackable pRib-AMP derivatives from Rib-A. An intriguing possibility is that TIR and TNL generated pRib-AMP is mobile through apoplast-cytoplasm exchange, thus contributing to systemic spread of immunity signals in leaves and the vasculature[46].

We attributed the enhanced potency and persistence of Thio-pRib-AMP compared to pRib-AMP in promoting *Arabidopsis* immune responses (Fig. 2b, c & EDF 3c) to increased Thio-pRib-AMP stability, as observed in leaf cell extracts (EDF. 3a, b), although more efficient Thio-pRib-AMP uptake into cells cannot be discounted. Thio-pRib-AMP binding properties were similar to those of pRib-AMP in ligand docking models (Fig. 2a) and thermal shift assays indicated that both molecules bind purified EDS1-PAD4 dimer (EDF. 4). The predicted hydrolytic instability of pRib-AMP might be a key rate-limiting step in EDS1-PAD4-ADR1 immune signalling[13,18]. A 50 nM – 100 nM Thio-pRib-AMP spray treatment in *Arabidopsis* reduced bacterial (*Pst*) and oomycete (*Hpa*) infections (Fig. 4), suggesting that Thio-pRib-AMP bioactivity is not limited by available EDS1-PAD4 dimer or ADR1-family proteins which execute the immune response. Some Thio-pRib-AMP might be pre-loaded onto the EDS1-PAD4 complex[21,47], thereby sensitizing cells for immune activation upon pathogen challenge. While the dynamics of Thio-pRib-AMP actions will require future study, phosphorothioate bonds[48,49] have been previously employed in approved drugs for human diseases[36,48], consistent with this chemical modification not being inherently toxic. Effectiveness of Thio-pRib-AMP low dose applications in reducing pathogen infection of *Arabidopsis*, *Nb* and *B. napus*

(Fig. 4, 5), suggest the small molecule treatment by-passes the need for specific pathogen recognition and thus could be used alone or in a formulation to augment natural defences against disease in a broad range of crops.

The described modular access to Rib-A as a common precursor provides a path for late-stage functionalization to alter EDS1-PAD4 affinity and signalling outputs, thereby expanding the accessible chemical space of bioactive second messenger analogues. Such diversification may enable fine control over immune stimulant potency, persistence, and biological context without altering the core pRib-AMP recognition motif. A deeper understanding of the structural parameters governing pRib-AMP activity, including its stereochemical features and phosphate contributions, will be essential to guide future optimization. This study positions ribosylated nucleotide scaffolds as a versatile platform for the development of next generation immune modulators.

Declarations

Conflict of Interest

A patent application for the preparation of pRib-AMP and related derivatives has been filed (EP25191966.8). SCLH and JS are involved in pre-commercial innovation activities with Max Planck Innovation through the Max!mize program based on the patent and the findings presented in the manuscript.

Accession Codes

CCDC 2541753 (SI2) and CCDC 2541754 (SI3) contain supplementary crystallographic data for this paper and can be obtained from Cambridge Crystallographic Data Centre (CCDC) at https://www.ccdc.cam.ac.uk/structures/. RNA-sequencing reads have been deposited in the European Nucleotide Archive (ENA) at EMBL-EBI under accession number PRJEB113848. Level 1 identification and mass spec raw data are available at ftp://MSV000102017@massive-ftp.ucsd.edu.

Acknowledgements

We thank Dr. Jörg Neudörfl for crystal structure analysis and Dr. Ohad Roth for providing *Pst* DC3000 ΔHopQ1-1. We further thank colleagues who kindly provided published *Arabidopsis* mutant lines. J.E.P and S.K.-S. acknowledge support from iHEAD (NRW Profilbildung ID: PB22-025A). S.C., J.S., F.L., J.E.P and SK.-S are supported by Deutsche Forschungsgemeinschaft (DFG) CRC 1403 - project number 414786233. J.S. and S.K.-S. thank DFG for funding through RTG2550/1 (project ID 411422114) and Germany´s Excellence Strategy – EXC-2048 – project ID 390686111. S.L.H.C acknowledges EU Marie Skłodowska-Curie NISP – 101154161 and EMBO ALTF 313–2024 funding. J.S. is funded through a

Kekulé fellowship from the Fonds der Chemischen Industrie. J.E.P. is supported by the Max Planck Society.

Materials and Methods

Chemicals and solvents for organic synthesis

Chemicals acquired commercially were used without further purification. Chemicals and solvents were obtained from Acros, Carbolution, Merck, Thermo Scientific, Sigma-Aldrich and BLD Pharm. Trimethyl phosphate and $POCl_3$ were distilled and dried over activated molecular sieves (3 Å). Dry solvents were purchased from suppliers in septum bottles over appropriate drying agents.

Cooling baths

For reactions requiring temperatures below room temperature, appropriate cooling baths were applied. In the case of 0°C, a RC 6 CS LAUDA cryostat was used. For temperatures of -15°C, a NaCl/ice bath was employed.

Nuclear magnetic resonance spectroscopy (NMR)

NMR spectra were recorded on a Bruker Avance III 499 (499.92 MHz) or a Bruker Avance II$^+$ 600 (600.20 MHz) machines at room temperature. Deuterated solvents ($CDCl_3$ and D_2O) were acquired from Deutero GmbH. Tetramethyl silane was used as an internal standard to reference ^{1}H-spectra (δ = 0 ppm). The carbon signal of $CDCl_3$ was used to reference ^{13}C-spectra (δ = 77.16 ppm). Coupling constants were measured and are reported in hertz (Hz). Multiplicities are reported as follows: singlet “s”, dublet “d”, triplet “t”, quartet “q”, pentet “p”, multiplet “m”. For the assignment of the signals 2D-NMR experiments (H,C-HMBC, H,C-HSQC and H,H-COSY) were carried out.

Fourier transformation infrared spectroscopy

Infrared spectra were performed on a Perkin-Elmer UTAR Two FT-IR spectrometer according to the method of attenuated total reflection (ATR). All spectra were recorded at room temperature. The wavenumbers are given in cm^{-1}. The signal intensity is indicated by the following abbreviations: w (weak), m (medium), s (strong). Strongly broadened signals are marked with the addition br (broad).

High resolution mass spectrometry (HR-MS)

HR-MS measurements were performed using electrospray ionization (ESI) on a THERMO Scientific LTQ Orbitrap XL machine. Nitrogen was used as carrier gas and a spray voltage of 3.2 kV was applied. An LTQ Orbitrap analyzer was used as mass selective detector.

Single crystal X-ray diffraction (SC-XRD)

SC-XRD measurements were performed on a SC-XRD Bruker D8 Venture at 100 K. Data analysis was carried out by Dr. J.-M. Neudörfl.

Thin layer chromatography (TLC)

Thin layer chromatography was performed using TLC Aluminum Plates by *VWR Europe* (specification film thickness: 200 µm), with a fluorescence indicator UV254 as solid phase. Visualization of compounds was performed by either UV-detection (254 nm) or staining with staining solutions. Aqueous $KMnO_4$ solution or ethanolic vanillin solution were used as staining solutions.

Column chromatography

Silica (60 Å, 0.035–0.070 mm) by *Acros Organics* was used as solid phase. The ratio of solvents in mobile phase are given in volume fraction. Flash chromatography was performed to increase the flow rate through a hand pump.

Reverse-phase preparative high-performance liquid chromatography (HPLC)

Purification by reverse phase preparative HPLC was performed using an *Interchim* puriFlash® 5.250P system. This system was equipped with an Interchim puriFlash® PF-30C18HP-F0040 as flash column. For the purification of phosphates, a puriFlash® Bio 100 PFB5C18-XS column was used. As mobile phase, a gradient of acetonitrile and aqueous 0.1 M formic acid for small molecules or aqueous 0.1 M triethyl ammonium bicarbonate (TEAB) for phosphates was used. The detection of analytes was conducted via an UV-detector at 254 nm.

Chemical synthesis

A comprehensive procedure for the chemical synthesis of the compounds used in this study is detailed in the Supplementary Information.

Arabidopsis materials and growth conditions

Arabidopsis thaliana ecotype Columbia-0 (Col-0) WT was used. Col-0 mutants and transgenic lines used in this study are listed in Supplementary table 3. To prepare seedlings for pRib-AMP treatments, seeds were germinated on ½ Murashige Skoog (MS) without sucrose under 16 h/8 h (light/dark) conditions with 100 µmol m^{-2} s^{-1} light intensity in a growth chamber. Eight-day-old seedlings were used for assays. To prepare soil-grown plants for protoplasts and leaves disease resistance assays, seeds were germinated on soil in a growth chamber and maintained under 8 h/16 h (light/dark) conditions at 22^{o}C.

Arabidopsis protoplast isolation and transfection

Soil grown 4–5-week-old *Arabidopsis* plants maintained at 8 h/16 h (light/dark) conditions were used for protoplast preparations according to described protocol[50]. Leaves were cut in strips with a surgical blade and treated with enzyme solution (20 mM MES (pH 5.7) containing 1.5% cellulase R-10 (SERVA),

0.4% macerozyme R-10 (SERVA), 0.4 M mannitol, 20 mM KCl, and 10 mM $CaCl_2$. Isolated protoplasts were washed in W5 solution (2 mM MES (pH 5.7) containing 154 mM NaCl, 125 mM $CaCl_2$ and 5 mM KCl) and resuspended in W5 for transfection. Lipofectamine 3000 transfection reagent (L3000; ThermoFisher Scientific) was used according to manufacturer's instructions. Briefly, TEA and pRib-AMP alone or complexed with L3000 were added to protoplast suspensions to a final concentration of 80 µM and 20 µM, respectively. Protoplasts were incubated for an additional 6–8 h and protoplast pellets were snap-frozen for RNA extraction.

Seedling pRib-AMP/Thio-pRib-AMP treatments and gene expression assays

Eight-day-old *Arabidopsis* seedlings were grown as described above. Test compounds were added to final concentration as indicated in ½ MS. A vacuum was applied for 3 mins followed by quick release. The infiltrated seedlings were transferred to 12-well plates with each well containing 10 to 15 seedlings in 2 ml ½ MS and incubated in the same growth chamber. Samples were harvested at indicated timepoints and snap-frozen for RNA extraction.

RNA extraction and reverse transcription-quantitative PCR (qRT-PCR)

Plant samples were homogenized and total RNA was extracted using a Zymo Research Direct-zol RNA miniprep kit with DNase following manufacturer's instructions. Extracted RNA concentrations in samples were quantified with nanodrop and RT was performed with iScript (Bio-Rad). Complementary DNA (cDNA) was diluted (1:5). qPCR assays were performed in a 96-well format using a Bio-Rad CFX96 real time system with cDNA, SyBR Green (Bio-Rad) and appropriate primer pairs. Primers for qRT-PCR are listed (Supplementary table 1).

Arabidopsis infection assays with Pst DC3000

Pst DC3000 with an empty vector (EV)[51] was utilized for infection assays. Plants were treated with indicated concentrations of TEA (mock), pRib-AMP or Thio-pRib-AMP by leaf infiltration or spraying onto leaves of fully expanded rosettes. Solutions used for leaf infiltration were in dH_20. Leaf spraying was performed by dissolving indicated concentrations of TEA and Thio-pRib-AMP in dH_20 containing 0.01% Tween-20 to solution run-off. Plants were then incubated for 1 d before challenge with *Pst* DC3000 in a growth chamber at 22^oC and 70% RH. *Pst* DC3000 (OD_{600} = 0.0005) in 10 mM $MgCl_2$ was syringe-infiltrated into fully expanded rosette leaves and bacterial titers (colony forming unit; CFU/cm^2) were determined at 3 d post infection (dpi) as described [21]. Each biological replicate consisted of two leaf disks from different leaves of one plant.

Arabidopsis infection assays with Hyaloperonospora arabidopsidis (Hpa) Noco2

Hpa isolate Noco2 (ref) was utilized for experiments on *Arabidopsis* accessions Ws-2 and Col-0. Three-week-old *Arabidopsis* plants were sprayed with indicated concentrations of TEA or Thio-pRib-AMP to

runoff and incubated for 1 d. *Hpa* Noco2 was then sprayed onto plants at 4 x 10^4 spores per ml H_2O. Spore counts and trypan blue staining were performed as described[42].

N. benthamiana infection assays with Pst DC3000 ΔHopQ

Five-week-old *N. benthamiana* plants grown at 26°C and16 h/8 h light/dark photoperiod were syringe infiltrated with mock (TEA, 4 µM) or Thio-pRib-AMP (0.5 µM) in dH_20. One d after infiltration, *Pst* DC3000 ΔHopQ1-1[45] cells were harvested from overnight cultures by centrifugation and resuspended in 10 mM $MgCl_2$. Bacterial suspensions were adjusted to an optical density at 600 nm (OD_{600}) of 0.4. Silwet L-77 was added to a final concentration of 0.02% (v/v) immediately prior to inoculation. After inoculation, plants were maintained under high humidity for 24 h and then transferred to standard growth conditions. Macroscopic disease symptoms were assessed at 6 dpi. For bacterial counting, leaf discs were collected at 0 and 6 dpi, homogenized in 10 mM $MgCl_2$, serially diluted, and plated on selective medium. CFUs were quantified after incubation at 28°C for 2 d.

Brassica napus infection assays with Pst DC3000

Brassica napus cultivar Vamos winter variety was acquired commercially from KWS (Einbeck, Germany). Plants were grown under a 12h/12h light/dark period at 22^oC (60% RH). Three-week-old plants were sprayed with indicated concentrations of TEA or Thio-pRib-AMP and incubated for 1 d. *Pst* DC3000 (OD_{600} = 0.1) was resuspended in 10 mM MgCl2 + 0.04% (v/v) Silwet L-77. Following inoculation, plants were maintained at high humidity for 24 h and then transferred to standard growth conditions. Bacterial titres and disease symptoms were measured at 3 dpi.

RNA-seq and analysis of expression data

RNA samples were sequenced by Novogene Europe by 150 sbp paired-end sequencing using the instrument Illumina NovaSeq X Plus. The qualities of the raw FASTQ reads were assessed by FastQC (http://www.bioinformatics.babraham.ac.uk/projects/fastqc) software. All reads were directly aligned to the *A. thaliana* genome TAIR10[52] with Araport11 gene annotations[53], using the STAR (v 2.7.11b) aligner[54]. Read counts for genes from the alignments were obtained with the featureCounts program from R package Rsubread (v 2.12.0)[55]. Differential expressions of genes were analysed by R package DESeq2 (v 1.38.0)[56] with the criteria of | log2 fold change | > 1.0 and false discovery rate adjusted p-value < 0.05. To cluster genes by expression patterns, a variance stabilizing normalisation was first applied to raw reads using the vst() function from DESeq2, followed by scale() function for Z-score normalization. Optimal number of clusters was determined using NbClust (v 3.0.1) R package[57], with silhouette score as index, euclidean distance and ward.D as the clustering method. Gene Ontology (GO) term enrichment analysis was performed with topGO (https://www.bioconductor.org/packages//2.7/bioc/vignettes/topGO/inst/doc/topGO.pdf), using Araport11 annotated GO terms as input. The heatmaps for differential expression were visualised by R package ComplexHeatmap (v 2.14.0)[58].

Arabidopsis ROS assays

Leaf discs of 4-week-old *Arabidopsis* WT plants were prepared using a 0.5 cm serological stamp and washed 3 times for 30 min with dH_2O. Leaf discs were transferred into wells of a white 96-well plate containing 100 µl dH_2O. After overnight incubation of plates in a growth chamber, the water was exchanged with elicitor solution. (20 µM L-012, 2 µg ml-1 HRP with indicated concentrations of pRib-AMP, 1 µM nlp20 or dH_2O (Mock). Luminescence was recorded for 1 h using a microplate luminometer (Centro, LB960).

Stability measurements of pRib-AMP and Thio-pRib-AMP in Arabidopsis lysates

Five-week-old WT *Arabidopsis* leaves were harvested, homogenized and resuspended in dH_2O (2 g/10 ml water). Suspensions were sonicated on ice at 40% amplitude, 15s/30s (on/off) for 15 cycles and incubated at 4 ^{o}C for 30 min. Homogenates were centrifuged at 4000 rpm and supernatants recovered. pRib-AMP or Thio-pRib-AMP was added to the lysate to a final concentration of 100 µM. The SM-spiked lysates were incubated at 1,500 rpm in thermomixer for 0, 30, 60, 120, 240, 480 min & 24 h at 22°C.

Samples were transferred to a vial and compound detection was conducted using IC-MS. Separation was performed with a Dionex Integrion HPIC System (Thermo Fisher) with a AS11-HC column (2 mm × 250 mm, Thermo Fisher) at 30°C. A guard column, Dionex Ionpac AG11-HC b (2 mm × 50 mm, Thermo Fisher), was placed before the separation column. The eluent (KOH) was generated in situ by a KOH cartridge and deionized water. A flow rate of 0.380 mL/min with gradient was used for the separation: 0–2 min 35 mM KOH, 2–6 min 35–100 mM, 6–8 min 100 mM, 8,01–13 min 35 mM. The Integrion was connected to QExactive mass spectrometer operating in negative ionization mode, scanning in Full-MS in a mass range between m/z 59–602 & PRM: Thio-pRib-AMP=ms2 of 590.0187@hcd45.00 [50.0000-620.0000]; pRib-AMP= ms2 of 558.0644@hcd45.00 [50.0000-590.0000]. Resolution was set at 17,500. Maximal injection time was set to 200 ms. HESI source operated with a spray voltage of 2.75 kV. Ion tube transfer capillary temperature was 350°C, sheath gas flow 50 arbitrary units (AU), auxiliary gas flow 14 AU, and sweep gas flow was set to 3 AU at 380°C. Level 1 identification data for pRib-AMP & Thio-pRib-AMP was provided (MSV000102017, confirming the structure by matching the main fragmentation of the reference standard using MS/MS and retention time. Data analysis was performed using the Quan module of Trace Finder 4.1 software (Thermo Fisher Scientific) in combination with a sample-specific compound database, derived from measurements of synthetized reference compounds.

Heterologous protein expression in insect cells

ExpiSF9 cell line (ThermoFisher Scientific) was utilized for insect cell expression. pFASTBAC containing the coding sequences of EDS1 and PAD4-Twin-strep (PAD4-TS) have been described[13]. Corresponding baculoviruses were obtained following manufacturer's instructions. Insect cell co-expression was performed by mixing the indicated baculoviruses at an equivalent ratio. Cells were harvested at 60 h post infection and lysed with 50 mM Tris HCl pH 8.0, 100 mM NaCl and 1 mM DTT. EDS1-PAD4-TS was

purified with Strep-Tactin XT (IBA Lifesciences) and separated by size exclusion chromatography (SEC) using Superdex 16/600 (Cytiva). Recombinant EDS1-PAD4-TS proteins were snap frozen in liquid N_2 after the addition of glycerol to 5% (v/v). Purified EDS1-PAD4-TS protein was verified by Coomassie blue, SEC and western blot.

Thermal shift assays (TSA)

The same batch of EDS1-PAD4-TS was utilized for TSA experiments. A final concentration of 5–10 µM EDS1-PAD4 dimer was incubated with 50 µM pRib-AMP or Thio-pRib-AMP for 30 min in 25 mM Tris HCl pH 8.0, 150 mM NaCl and 1 mM DTT at RT. SYPRO Orange (Catalog number, S6650; ThermoFisher Scientific) was added according to manufacturer's instructions. Melting curves were measured in a 96-well format using a Bio-Rad CFX96 real time system from 25 to 95°C in increments of 0.5°C. Data was fitted by MoltenProt v1.1, and unfolded fraction data was used to estimate Tm value by Boltzmann sigmoidal equation in Graph Pad Prism version 5.00 (La Jolla California, USA) using the normalization function[59].

R packages and figure formatting programs used in this study

Data analysis and visualization was performed in R (version 4.3.3; R Foundation for Statistical Computing, Vienna). The following R packages were used: ggplot2 (https://ggplot2.tidyverse.org; 3.5.0); plyr (https://www.jstatsoft.org/v40/i01/; 1.8.9); lattice (http://lmdvr.r-forge.r-project.org; 0.22.6); Rmisc (https://CRAN.R-project.org/package=Rmisc; 1.5.1); ggbreak[60]; multcompView (https://CRAN.R-project.org/package=multcompView; 0.1.10). Final figure formatting was carried out using Adobe Illustrator (version 28.4.1, Adobe Inc.).

EDF 2. pRib-AMP induced transcriptional reprogramming is independent of Arabidopsis pattern recognition and signalling components. (a)

pRib-AMP induced defence marker gene expression in 8-day-old WT, *rbohD, bak1/bkk1, btl2*, *mik2, bak1/bkk1/btl2*, AEQ (aequorine) WT and *dorn1* (in AEQ background) (see Supplementary table 3 for mutant details), treated with 80 µM Triethylammonium (counterion, TEA; –) or 20 µM TEA_4pRib-AMP (+) for 6 h. Relative expression was normalized to *ACTIN2* and set to WT (–) samples. Bars indicate mean expression ± s.e.m. (n:3 biological replicates, indicated by different shapes from one independt epxeriment). Asterisks indicate statistically significant differences according to two-tailed Student T-test. *:$P < 0.05$; **:$P < 0.005$; ***:$P < 0.0005$: ns: non-significant, $P > 0.05$. A second independent experiment gave similar results. **(b)** Quantification of ROS production in leaf discs of 4-week-old WT plants. Leaf discs were treated with mock (400 µM TEA) or 1, 20 or 100 µM TEA_4pRib-AMP, and 1 µM nlp20 elicitor as a positive control. ROS was measured by a luminescence reporter for 60 min. Data points represent a

pool of 8 leaf discs. Two independent experiments, each with 2 biological replicates (n: 2), gave similar results. Error bars represent standard deviation (SD).

EDF 3. Comparative stability, potency and sustained action of pRib-AMP and Thio-pRib-AMP in Arabidopsis. (a)

Schematic of the pRib-AMP and Thio-pRib-AMP compound stability assay. 100 µM of TEA_4pRib-AMP or TEA_4Thio-pRib-AMP was added into a leaf lysate derived from 4-week-old WT plants, incubated at 22^{o}C and then processed for LC-MS quantitation at time points indicated in (b). **(b)** Relative abundance of pRib-AMP (left) and Thio-pRib-AMP (right). Results are normalized to 0 h levels of each molecule. Data are means ± SD (n:1 biological replicate each timepoint from two independent experiments). **(c)** Eight-day-old seedlings of WT and *pad4* were vacuum infiltrated with 80 µM Triethylammonium (counterion, TEA; –), 20 µM TEA_4pRib-AMP (pRib-AMP) or 20 µM TEA_4Thio-pRib-AMP (Thio-pRib-AMP) for 6 h (upper panel) and 12 h (bottom panel) before processing for defence gene expression analyses. Bars indicate mean expression ± s.e.m. (n:4 biological replicates from two independent experiments, indicated by different shapes). Different letters indicate statistically significant difference (FDR:0.05) determined by Kruskal–Wallis with post-hoc two-sided pairwise comparisons using Wilcoxon rank sum test. For three replicates, data were taken from Fig. 2b, excluding treatments with mono-Et-pRib-AMP.

EDF 4. Thermal shift assay (TSA) of EDS1-PAD4 with pRib-AMP or Thio-pRib-AMP. (a)

TSA curves of Apo-EDS1-PAD4 (black), EDS1-PAD4 + pRib-AMP (blue), EDS1-PAD4 + Thio-pRib-AMP (green). 10 µM EDS1-PAD4 was added with 50 µM of either TEA_4pRib-AMP or TEA_4Thio-pRib-AMP. Data are means ± SD. n:3 (technical replicates). **(b)** Table representing melting temperature (T_m) of each setup from two independent experiments.

EDF 5. Gene ontology (GO) term analysis of Thio-pRib-AMP response in Arabidopsis WT and pad4 seedlings at 6 h. (a)

GO term analysis of down-regulated differential expressed genes (DEG) in WT, corresponding to WT-only 1357 DEG in Fig. 3c. **(b)** GO term analysis of up-regulated DEG in *pad4* corresponding to *pad4*-only 532 DEG in Fig. 3b. **(c)** GO term analysis of down-regulated DEG in *pad4*, corresponding to *pad4*-only 778 DEG in Fig. 3c.

EDF 6. Thio-pRib-AMP up-regulated Arabidopsis immune-related DEG compared to TNL RRS1/RPS4 immune response to Pst-avrRps4 bacteria.

The heatmap shows up-regulated DEG by 100 nM TEA_4Thio-pRib-AMP treatment (+) compared to mock treatment (–) at 6h in WT RNA-seq analysis (column #1). Genes were taken from Supplementary table 2 (WT_6hr_MockVSThio_DEGs) corresponding to 2369 up-regulated DEG in WT, and categorized into immune-related functions. Differential expression of these genes is compared with a published RNA-seq

analysis of Col WT plants relative to Col *eds1* plants at 8 h post inoculation with *Pst* DC3000 *Avr*RPS4 (A4) (panel #2)[39].

EDF 7. Schematics of Arabidopsis Thio-pRib-AMP treatments and infection assays with Pst DC3000 and Hpa Noco2 in Fig. 4. (a)

Four-week-old *Arabidopsis* Col-0 (WT) and *pad4* plants were sprayed with 400 nM Triethylammonium [counterion, TEA; (–)] or corresponding doses of TEA_4Thio-pRib-AMP. Plant fresh weights were measured at 8 d post spraying. **(b)** Five-week-old *Arabidopsis* WT and *pad4* plants were sprayed with 400 nM TEA or corresponding doses of TEA_4Thio-pRib-AMP. After 1 day, leaves were infiltrated with *Pst* DC3000 (OD:0.0005). Colony forming units (CFUs) were measured at 3 d post infiltration (dpi), and macroscopic disease symptoms were recorded at 6 dpi. **(c)** Two-week-old Arabidopsis accession Ws-2 (resistant), Col-0 (susceptible; WT) and *pad4* (hyper-susceptible) plants were sprayed with 200 nM TEA, 50 nM or 100 nM TEA_4Thio-pRib-AMP. After 1 d, *Hpa* Noco2 was spray-inoculated onto leaves. Conidiospore counting and trypan blue staining to detect Noco2 hyphae and plant host reactions were monitored at 5 dpi.

References

1. Köninger J et al (2026) Pesticide residues alter taxonomic and functional biodiversity in soils. Nature. https://doi.org:10.1038/s41586-025-09991-z
2. Wolfram J et al (2026) Increasing applied pesticide toxicity trends counteract the global reduction target to safeguard biodiversity. Science 391:616–621. https://doi.org:10.1126/science.aea8602
3. Wan NF et al (2025) Pesticides have negative effects on non-target organisms. Nat Commun 16:1360. https://doi.org:10.1038/s41467-025-56732-x
4. Ma CS et al (2021) Climate warming promotes pesticide resistance through expanding overwintering range of a global pest. Nat Commun 12:5351. https://doi.org:10.1038/s41467-021-25505-7
5. Schriever C et al (2025) The European regulatory system for plant protection products-cause of a Silent Spring or highly advanced and protective? Integr Environ Assess Manag 21:3–19. https://doi.org:10.1093/inteam/vjae007
6. Schneider K, Barreiro-Hurle J, Rodriguez-Cerezo E (2023) Pesticide reduction amidst food and feed security concerns in Europe. Nat Food 4:746–750. https://doi.org:10.1038/s43016-023-00834-6
7. Ngou BPM, Ding P, Jones JDG (2022) Thirty years of resistance: Zig-zag through the plant immune system. Plant Cell 34:1447–1478. https://doi.org:10.1093/plcell/koac041
8. Hu Z, Chai J (2023) Assembly and Architecture of NLR Resistosomes and Inflammasomes. Annu Rev Biophys 52:207–228. https://doi.org:10.1146/annurev-biophys-092922-073050
9. Jones JDG, Staskawicz BJ, Dangl JL (2024) The plant immune system: From discovery to deployment. Cell 187:2095–2116. https://doi.org:10.1016/j.cell.2024.03.045

10. Locci F, Parker JE (2024) Plant NLR immunity activation and execution: a biochemical perspective. Open Biol 14:230387. https://doi.org:10.1098/rsob.230387
11. Ngou BPM et al (2025) Systematic discovery and engineering of synthetic immune receptors in plants. Science 389:eadx2508. https://doi.org:10.1126/science.adx2508
12. Zdrzalek R, Stone C, De la Concepcion JC, Banfield MJ, Bentham AR (2023) Pathways to engineering plant intracellular NLR immune receptors. Curr Opin Plant Biol 74:102380. https://doi.org:10.1016/j.pbi.2023.102380
13. Huang S et al (2022) Identification and receptor mechanism of TIR-catalyzed small molecules in plant immunity. Science 377:eabq3297. https://doi.org:10.1126/science.abq3297
14. Jia A et al (2022) TIR-catalyzed ADP-ribosylation reactions produce signaling molecules for plant immunity. Science 377:eabq8180. https://doi.org:10.1126/science.abq8180
15. Ma S et al (2020) Direct pathogen-induced assembly of an NLR immune receptor complex to form a holoenzyme. Science 370. https://doi.org:10.1126/science.abe3069
16. Martin R et al (2020) Structure of the activated ROQ1 resistosome directly recognizing the pathogen effector XopQ. Science 370. https://doi.org:10.1126/science.abd9993
17. Essuman K, Milbrandt J, Dangl JL, Nishimura MT (2022) Shared TIR enzymatic functions regulate cell death and immunity across the tree of life. Science 377:eabo0001. https://doi.org:10.1126/science.abo0001
18. Yu H et al (2024) Activation of a helper NLR by plant and bacterial TIR immune signaling. Science 386:1413–1420. https://doi.org:10.1126/science.adr3150
19. Bayless AM et al (2023) Plant and prokaryotic TIR domains generate distinct cyclic ADPR NADase products. Sci Adv 9:eade8487. https://doi.org:10.1126/sciadv.ade8487
20. Song W et al (2024) Substrate-induced condensation activates plant TIR domain proteins. Nature 627:847–853. https://doi.org:10.1038/s41586-024-07183-9
21. Pruitt RN et al (2021) The EDS1-PAD4-ADR1 node mediates Arabidopsis pattern-triggered immunity. Nature 598:495–499. https://doi.org:10.1038/s41586-021-03829-0
22. Tian H et al (2021) Activation of TIR signalling boosts pattern-triggered immunity. Nature 598:500–503. https://doi.org:10.1038/s41586-021-03987-1
23. Dongus JA et al (2022) Cavity surface residues of PAD4 and SAG101 contribute to EDS1 dimer signaling specificity in plant immunity. Plant J 110:1415–1432. https://doi.org:10.1111/tpj.15747
24. Wu Y et al (2024) A canonical protein complex controls immune homeostasis and multipathogen resistance. Science 386:1405–1412. https://doi.org:10.1126/science.adr2138
25. Johanndrees O et al (2023) Variation in plant Toll/Interleukin-1 receptor domain protein dependence on ENHANCED DISEASE SUSCEPTIBILITY 1. Plant Physiol 191:626–642. https://doi.org:10.1093/plphys/kiac480
26. Lapin D, Johanndrees O, Wu Z, Li X, Parker JE (2022) Molecular innovations in plant TIR-based immunity signaling. Plant Cell 34:1479–1496. https://doi.org:10.1093/plcell/koac035

27. Sun X et al (2021) Pathogen effector recognition-dependent association of NRG1 with EDS1 and SAG101 in TNL receptor immunity. Nat Commun 12:3335. https://doi.org:10.1038/s41467-021-23614-x
28. Xiao Y et al (2025) Activation and inhibition mechanisms of a plant helper NLR. Nature 639:438–446. https://doi.org:10.1038/s41586-024-08517-3
29. Huang S et al (2025) Balanced plant helper NLR activation by a modified host protein complex. Nature 639:447–455. https://doi.org:10.1038/s41586-024-08521-7
30. Peng K, Anmangandla A, Jana S, Jin Y, Lin H (2024) Iso-ADP-Ribose Fluorescence Polarization Probe for the Screening of RNF146 WWE Domain Inhibitors. ACS Chem Biol 19:300–307. https://doi.org:10.1021/acschembio.3c00512
31. Mikhailov SN et al (1997) An Efficient Synthesis and Physico-Chemical Properties OF 2'-O-d-Ribofuranosylnuleosides, Minor tRNA Components. J Carbohydr Chem 16:75–92. https://doi.org:10.1080/07328309708006511
32. Liu W et al (2020) Lipofection-mediated genome editing using DNA-free delivery of the Cas9/gRNA ribonucleoprotein into plant cells. Plant Cell Rep 39:245–257. https://doi.org:10.1007/s00299-019-02488-w
33. Bonardi V et al (2011) Expanded functions for a family of plant intracellular immune receptors beyond specific recognition of pathogen effectors. Proc Natl Acad Sci U S A 108:16463–16468. https://doi.org:10.1073/pnas.1113726108
34. Dong OX et al (2016) TNL-mediated immunity in Arabidopsis requires complex regulation of the redundant ADR1 gene family. New Phytol 210:960–973. https://doi.org:10.1111/nph.13821
35. Lapin D et al (2019) A Coevolved EDS1-SAG101-NRG1 Module Mediates Cell Death Signaling by TIR-Domain Immune Receptors. Plant Cell 31:2430–2455. https://doi.org:10.1105/tpc.19.00118
36. Elliott TS, Slowey A, Ye Y, Conway SJ (2012) The use of phosphate bioisosteres in medicinal chemistry and chemical biology. MedChemComm 3:735–751. https://doi.org:10.1039/c2md20079a
37. Nassir M, Isaak A, Fischer B (2022) Hydrolytic (in)stability of phosphate isosteres. Eur J Med Chem 244:114836. https://doi.org:10.1016/j.ejmech.2022.114836
38. Khan MF et al (2024) Determination of Protein-Ligand Binding Affinities by Thermal Shift Assay. ACS Pharmacol Transl Sci 7:3096–3107. https://doi.org:10.1021/acsptsci.4c00293
39. Bhandari DD et al (2019) An EDS1 heterodimer signalling surface enforces timely reprogramming of immunity genes in Arabidopsis. Nat Commun 10:772. https://doi.org:10.1038/s41467-019-08783-0
40. Hartmann M et al (2018) Flavin Monooxygenase-Generated N-Hydroxypipecolic Acid Is a Critical Element of Plant Systemic Immunity. Cell 173:456–469. https://doi.org:10.1016/j.cell.2018.02.049.e416
41. Ngou BPM, Ahn HK, Ding P, Jones JDG (2021) Mutual potentiation of plant immunity by cell-surface and intracellular receptors. Nature 592:110–115. https://doi.org:10.1038/s41586-021-03315-7

42. Stuttmann J et al (2011) Perturbation of Arabidopsis amino acid metabolism causes incompatibility with the adapted biotrophic pathogen Hyaloperonospora arabidopsidis. Plant Cell 23:2788–2803. https://doi.org:10.1105/tpc.111.087684
43. Gantner J, Ordon J, Kretschmer C, Guerois R, Stuttmann J (2019) An EDS1-SAG101 Complex Is Essential for TNL-Mediated Immunity in. Plant Cell 31:2456–2474. https://doi.org:10.1105/tpc.19.00099
44. Qi T et al (2018) NRG1 functions downstream of EDS1 to regulate TIR-NLR-mediated plant immunity in Nicotiana benthamiana. Proc Natl Acad Sci U S A 115. https://doi.org:10.1073/pnas.1814856115. E10979-E10987
45. Wang H et al (2024) The NLR immune receptor ADR1 and lipase-like proteins EDS1 and PAD4 mediate stomatal immunity in Nicotiana benthamiana and Arabidopsis. Plant Cell 36:427–446. https://doi.org:10.1093/plcell/koad270
46. Tang B, Feng L, Hulin MT, Ding P, Ma W (2023) Cell-type-specific responses to fungal infection in plants revealed by single-cell transcriptomics. Cell Host Microbe 31:1732–1747e1735. https://doi.org:10.1016/j.chom.2023.08.019
47. Fliegmann J et al (2025) Canonical EDS1/PAD4 small-molecule binding sites are required for LRR-RP-mediated pattern-triggered immunity. *Proc. Natl. Acad. Sci. U.S.A.* 123 (25) e2536973123 https://doi.org/10.1073/pnas.2536973123
48. Eckstein F, Phosphorothioates (2014) Essential Components of Therapeutic Oligonucleotides. Nucleic Acid Ther 24:374–387. https://doi.org:10.1089/nat.2014.0506
49. Gish G, Eckstein F (1988) DNA and RNA sequence determination based on phosphorothioate chemistry. Science 240:1520–1522. https://doi.org:10.1126/science.2453926
50. Yoo SD, Cho YH, Sheen J (2007) Arabidopsis mesophyll protoplasts: a versatile cell system for transient gene expression analysis. Nat Protoc 2:1565–1572. https://doi.org:10.1038/nprot.2007.199
51. Century KS, Holub EB, Staskawicz BJ (1995) NDR1, a locus of Arabidopsis thaliana that is required for disease resistance to both a bacterial and a fungal pathogen. Proc Natl Acad Sci U S A 92:6597–6601. https://doi.org:10.1073/pnas.92.14.6597
52. Lamesch P et al (2012) The Arabidopsis Information Resource (TAIR): improved gene annotation and new tools. Nucleic Acids Res 40:D1202–1210. https://doi.org:10.1093/nar/gkr1090
53. Cheng CY et al (2017) Araport11: a complete reannotation of the Arabidopsis thaliana reference genome. Plant J 89:789–804. https://doi.org:10.1111/tpj.13415
54. Dobin A et al (2013) STAR: ultrafast universal RNA-seq aligner. Bioinformatics 29:15–21. https://doi.org:10.1093/bioinformatics/bts635
55. Liao Y, Smyth GK, Shi W (2014) featureCounts: an efficient general purpose program for assigning sequence reads to genomic features. Bioinformatics 30:923–930. https://doi.org:10.1093/bioinformatics/btt656

56. Love MI, Huber W, Anders S (2014) Moderated estimation of fold change and dispersion for RNA-seq data with DESeq2. Genome Biol 15:550. https://doi.org:10.1186/s13059-014-0550-8
57. Charrad M, Ghazzali N, Boiteau V, Niknafs A, Nbclust (2014) An R Package for Determining the Relevant Number of Clusters in a Data Set. J Stat Softw 61:1–36
58. Gu Z, Eils R, Schlesner M (2016) Complex heatmaps reveal patterns and correlations in multidimensional genomic data. Bioinformatics 32:2847–2849. https://doi.org:10.1093/bioinformatics/btw313
59. Zhang Z et al (2016) Crystal structure of unlinked NS2B-NS3 protease from Zika virus. Science 354:1597–1600. https://doi.org:10.1126/science.aai9309
60. Xu S et al (2021) Use ggbreak to Effectively Utilize Plotting Space to Deal With Large Datasets and Outliers. Front Genet 12:774846. https://doi.org:10.3389/fgene.2021.774846

Figures

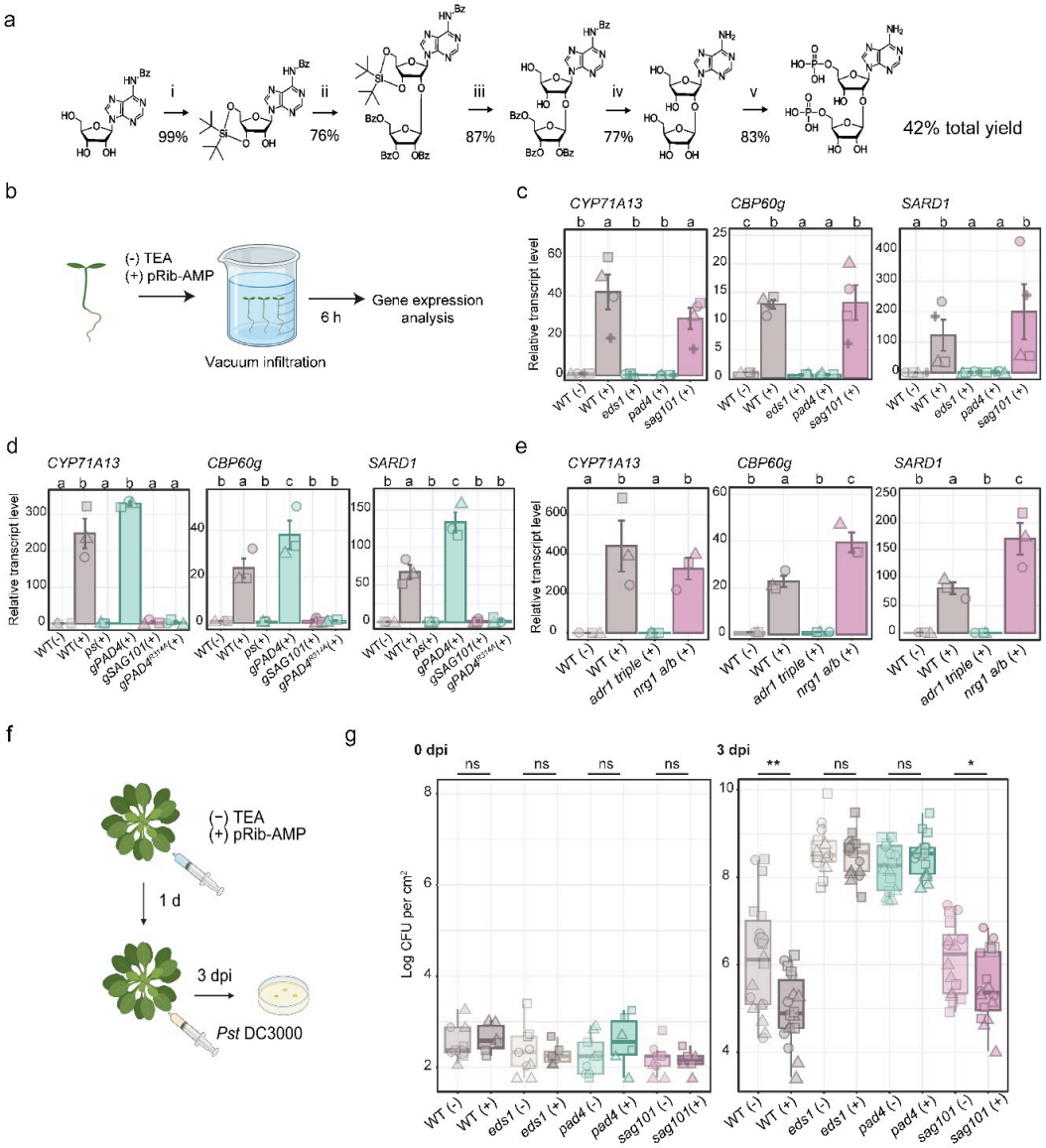


Figure 1. pRib-AMP synthetic route and *in vivo* immune-stimulating activity.

Figure 1

pRib-AMP synthetic route and in vivo immune-stimulating activity assay. (a) Schematic representation of the chemical synthetic route to pRib-AMP. Reaction steps are denoted as i-iv (above arrow) and % yield at each step is indicated (below arrow). **(b)** Scheme for *Arabidopsis* seedling treatments with pRib-AMP and transcriptional response assays shown in panels (c), (d) and (e). Eight-day-old-seedlings were vacuum infiltrated with 80 µM Triethylammonium (counterion, TEA (−) or 20 µM TEA_4pRib-AMP (+) and

incubated for 6 h before gene expression analysis shown in **(c)** WT, *eds1*, *pad4* and *sag101* **(d)** WT, *pad4sag101* (*ps*), *gPAD4/ps, gSAG101/ps* and *gPAD4*^{R314A}*/ps*, and **(e)** WT, *adr1 triple, nrg1 a/b*. Relative expression was normalized to *ACTIN2* and set to mock WT (-) samples. Bars indicate mean expression ± s.e.m. (n:3 biological replicates from one independent experiment, indicated by different shapes). Different letters indicate statistically significant difference (FDR:0.05) determined by (c) Kruskal–Wallis with post-hoc two-sided pairwise comparisons using Wilcoxon rank sum test or (d) and (e) one-way ANOVA followed by Tukey's HSD. A second independent experiment gave similar results. **(f)** Scheme for pRib-AMP infiltration into *Arabidopsis* 4-week-old plants to monitor disease resistance against virulent *Pseudomonas syringae pv tomato (Pst)* DC3000. **(g)** *Pst* DC3000 titers in WT, *eds1, pad4* and *sag101* plants syringe-infiltrated with 80 µM TEA (–) or 20 µM TEA_4-pRib-AMP (+). Bacteria colony forming units (CFU) were counted at 0 and 3 d post inoculation (dpi). Different shapes indicate independent experiments (n:3 or 6 biological replicates each for 0 and 3 dpi, respectively). Asterisks indicate *: $P<0.05$; **: $P<0.005$; non-significant (ns): $P>0.05$ according to two-tailed Student t-test. For box plots, the centre line indicates the median, the bounds of the box show the 25th and the 75th percentiles, and the whiskers indicate 1.5 × IQR.

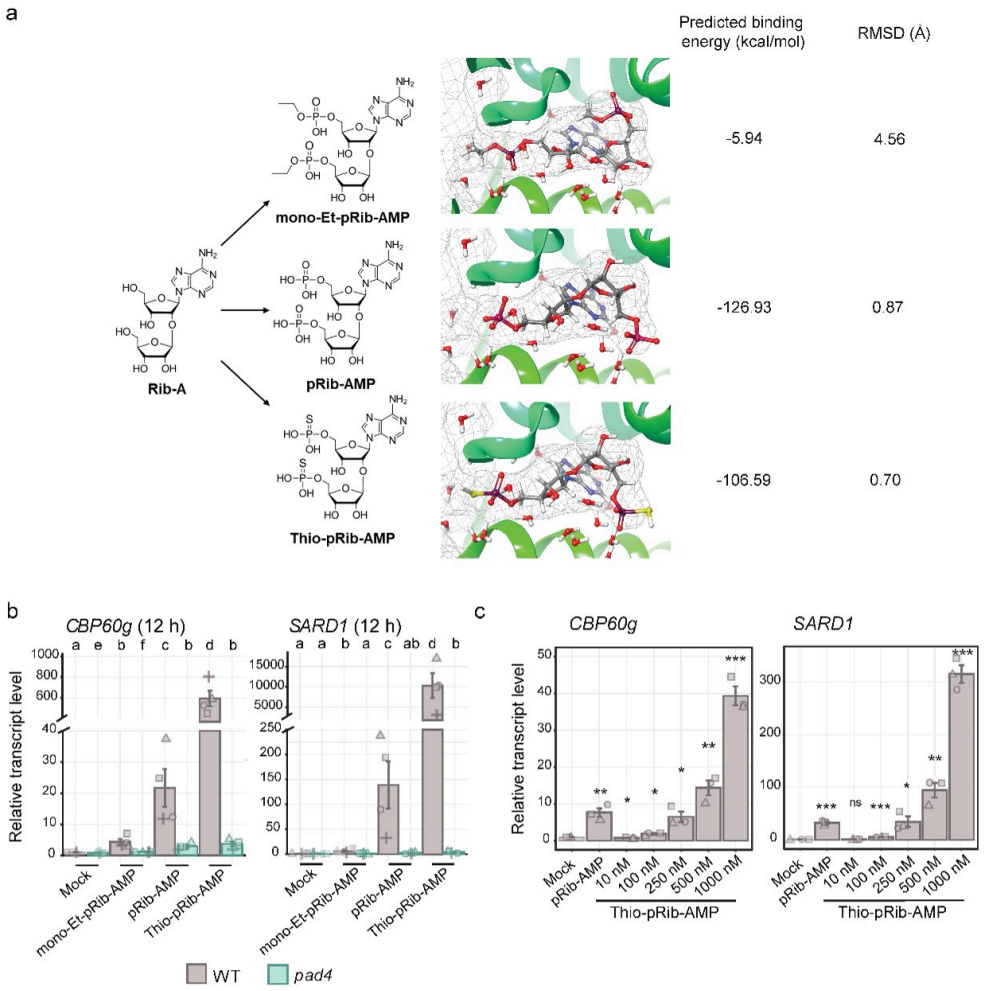


Figure 2. Chemical derivatization and functional characterization of Thio-pRib-AMP.

Figure 2

Chemical derivatization and functional characterization of Thio-pRib-AMP. (a) Schematic of chemical derivatization from Ribose-Adenosine (Rib-A) to mono-Et-pRib-AMP, pRib-AMP or Thio-pRib-AMP (left panel). Molecular docking of the above ligands to the binding pocket of EDS1-PAD4 (middle panel). Predicted binding energy (kcal/mol) and root mean square deviation (RMSD) of each predicted ligand EDS1-PAD4 complex is reported in Å (right panel). **(b)** Eight-day-old *Arabidopsis* WT and *pad4* seedlings

were vacuum infiltrated with 80 µM Triethylammonium (counterion, TEA; Mock), 20 µM TEA_2mono-Et-pRib-AMP (mono-Et-pRib-AMP), 20 µM TEA_4pRib-AMP (pRib-AMP) or 20 µM TEA_4Thio-pRib-AMP (Thio-pRib-AMP) for 12 h before gene expression analysis. Bars indicate mean expression ± s.e.m. (n:4 biological replicates from two independent experiments, indicated by different shapes). Different letters indicate statistically significant difference (FDR:0.05) determined by Kruskal–Wallis with post-hoc two-sided pairwise comparisons using Wilcoxon rank sum test. **(c)** Eight-day-old WT seedlings were vacuum infiltrated with 80 µM Triethylammonium (counterion, TEA; Mock), 20 µM TEA_4pRib-AMP (pRib-AMP) or TEA_4Thio-pRib-AMP (Thio-pRib-AMP) at the indicated concentrations for 6 h before gene expression analysis. Bars indicate mean expression ± s.e.m. (n:3 biological replicates from one independent experiment, indicated by different shapes). Asterisks indicate *: $P<0.05$; **: $P<0.005$; ***:$P<0.0005$; non-significant (ns): $P>0.05$ according to two-tailed Student t-test. A second independent experiment gave similar results.

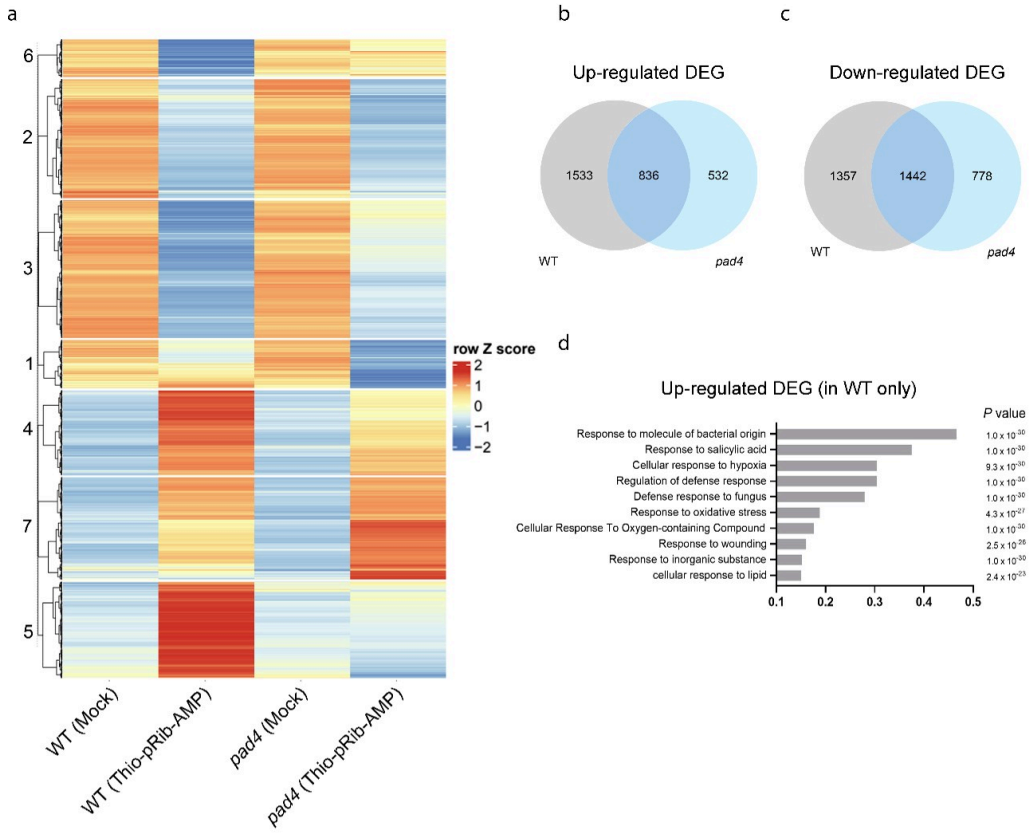


Figure 3. Transcriptomic analysis of Thio-pRib-AMP treatment in *Arabidopsis*.

Figure 3

Transcriptomic analysis of Thio-pRib-AMP treatment in *Arabidopsis*. (a) A heatmap representation of gene expression clusters from RNA-seq analysis of 8-day-old WT and *pad4* seedlings treated with 80 µM TEA (Mock) or 100 nM TEA_4Thio-pRib-AMP (Thio-pRib-AMP) for 6 h. The heatmap shows normalized expression Z scores for each row. Differentially expressed genes (DEG) with a false discovery rate (FDR) < 0.01 were used in the analysis; n: 3 biological replicates per genotype/treatment. Each replicate

contained 10-12 seedlings. **(b)** Venn diagram illustrating up-regulated DEG by 100 nM TEA_4Thio-pRib-AMP in WT and *pad4* compared to corresponding mock treatments. **(c)** Venn diagram illustrating down-regulated DEG by 100 nM Thio-pRib-AMP in WT and *pad4* compared to corresponding mock treatments. **(d)** Gene ontology (GO) analysis of up-regulated DEG in WT but not *pad4* after treatment with TEA_4Thio-pRib-AMP. The top 10 GO terms represented in WT-only 1533 DEG in panel (b) are displayed.

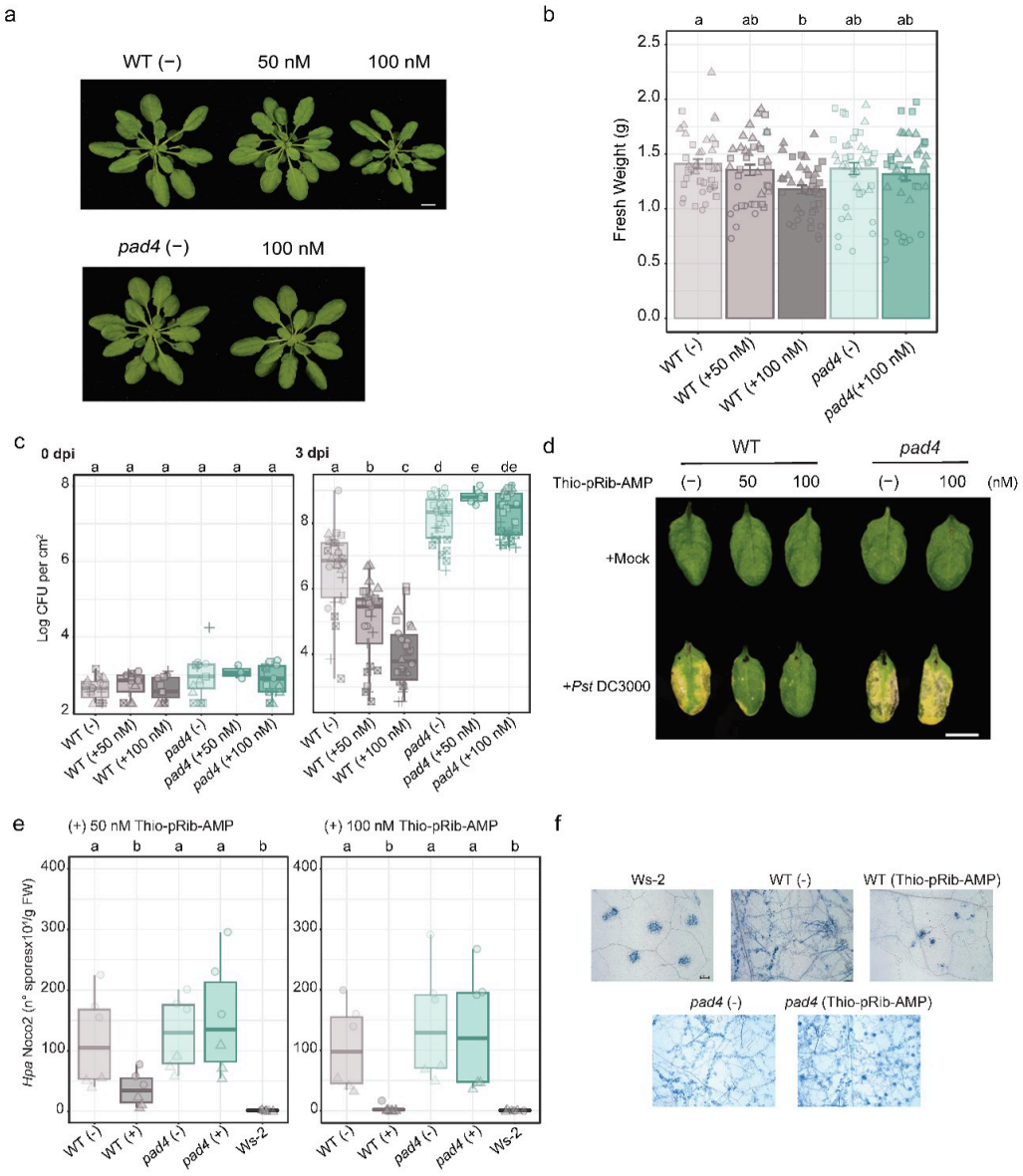


Figure 4. A low dose spray treatment of Thio-pRib-AMP promotes disease resistance in *Arabidopsis*.

Figure 4

A low dose spray treatment of Thio-pRib-AMP promotes disease resistance in *Arabidopsis*. (a) Development of 4-week-old Col-0 (WT) and *pad4* plants 8 d after spraying with 400 nM Triethylammonium (counterion, TEA; –), 50 nM or 100 nM TEA_4Thio-pRib-AMP. Scale bar: 1 cm. Plants shown are representative of n:16 per genotype assessed in three independent experiments. **(b)** Fresh weight measurements (g) of plants derived from (a). Different shapes indicate independent experiments. Bars indicate mean expression ± s.e.m. (n:8 or 16 per experiment). Different letters indicate statistically significant difference (FDR:0.05) determined by one-way ANOVA followed by Tukey's HSD. **(c)** *Pst* DC3000 titers in 4-week-old WT and *pad4* plants sprayed with 400 nM TEA (–), 50 nM or 100 nM TEA_4Thio-pRib-AMP (+) 1 d prior to *Pst* DC3000 syringe inoculation. Bacteria colony forming units (CFU) were counted at 0- and 3-d post inoculation (0 and 3 dpi). Different shapes indicate independent experiments (n:3 or 6 biological replicates each for 0 and 3 dpi). Different letters indicate statistically significant difference (FDR:0.05) determined by Kruskal–Wallis with post-hoc two-sided pairwise comparisons using Wilcoxon rank sum test. **(d)** Disease symptoms of representative leaves derived from (c) collected at 6 dpi. Scale bar: 1 cm. n:6 leaves per genotype from three independent experiments. **(e)** Infection phenotypes of 2-week-old WT, *pad4* and Ws-2 plants inoculated with *Hpa* isolate Noco2 1d after spraying leaves with water, 200 nM TEA (–), 50 nM (+, left panel) or 100 nM (+, right panel) TEA_4Thio-pRib-AMP. Pathogen spores on leaves were counted at 5 d after spray-inoculation with 4×10^4 spores ml–1. (n:3 biological replicates, comprising 30 plants each, in 2 two independent experiments). Different shapes indicate independent experiments (n:3 biological replicates in each). Different letters indicate statistically significant difference (FDR:0.05) determined by either one-way ANOVA followed by Tukey's HSD test (for 50 nM) or Kruskal–Wallis with post-hoc two-sided pairwise comparisons using Wilcoxon rank sum test (for 100 nM). **(f)** Trypan blue staining of leaves derived from (e) treated with 200 nM TEA (–) or 50 nM Thio-pRib-AMP. Scale bar: 100 µm. Images are representative of two independent experiments (one representative photo taken from 8-12 *Hpa*-infected leaves. For box plots (panels (c) and (e)), the centre line indicates the median, the bounds of the box show the 25^{th} and the 75^{th} percentiles, and the whiskers indicate 1.5 × IQR. See EDF. 7 for schematics of SM treatment and pathogen inoculation regimes.

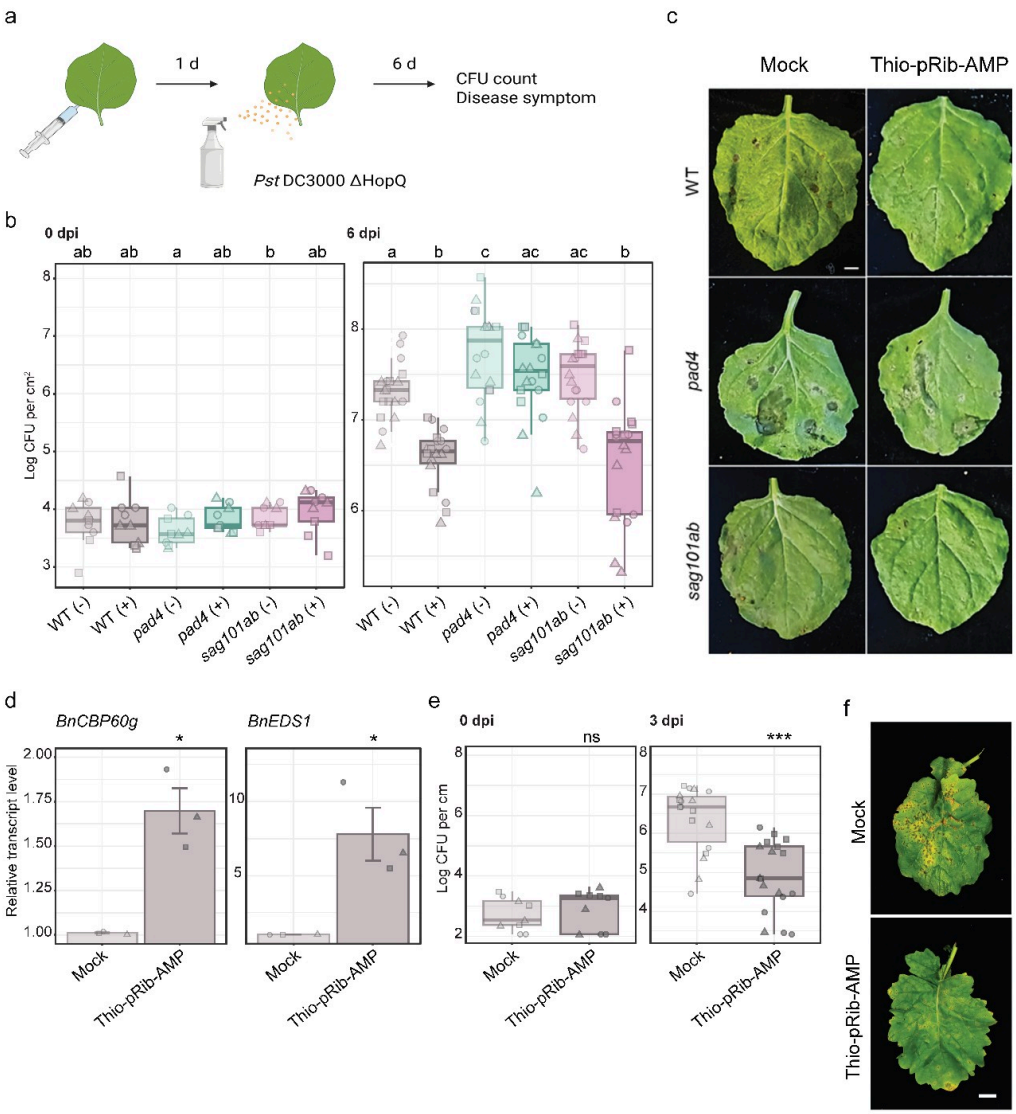


Figure 5. Thio-pRib-AMP application reduces bacterial infections in *Nicotiana benthamiana* and *Brassica napus.*

Figure 5

Thio-pRib-AMP application reduces bacterial infections in *Nicotiana benthamiana* and *Brassica napus*. **(a)** Scheme for Thio-pRib-AMP treatment of *N. benthamiana* leaves to protect against infection by virulent *Pst* DC3000 ΔHopQ1-1. **(b)** *Pst* DC3000 ΔHopQ1-1 titers in 5-week-old WT, *pad4* and *sag101ab* plants syringe-infiltrated with 2 µM TEA (–) or 500 nM TEA_4Thio-pRib-AMP (+). Bacteria colony forming units (CFU) were counted at 0 and 6 d post inoculation (0 and 6 dpi). Different shapes indicate

independent experiments (n:3 or 6 biological replicates each for 0 and 6 dpi). Different letters indicate statistically significant difference (FDR:0.05) determined by Kruskal–Wallis with post-hoc two-sided pairwise comparisons using Wilcoxon rank sum test. For box plots, the center line indicates the median, the bounds of the box show the 25th and the 75th percentiles, and the whiskers indicate 1.5 × IQR. **(c)** Disease symptoms of *N. benthamiana* leaves derived from (b) at 6 dpi. Pictures are representative of three independent experiments. Scale bar: 1 cm. **(d**) Induction of *BnCBP60g* and *BnEDS1* defence marker genes in 3-week-old WT *Brassica napus* cultivar Vamos leaves. Plants were treated with 400 nM Triethylammonium (counterion, TEA; –) or 100 nM TEA$_4$Thio-pRib-AMP (+) and incubated for 6 h before gene expression analyses. Relative expression was normalized to *BnACTIN2* and mock (–) samples for each treatment. Bars indicate mean expression ± s.e.m. (n:3 biological replicates from 1 experiment are indicated by different shapes). Asterisks indicate statistically significant differences according to a two-tailed Student T-test. *:*P*<0.05. A second independent experiment gave similar results. **(e)** *Pst* DC3000 titers in 4-week-old *Brassica napus* WT plants sprayed with 400 nM TEA (Mock) or 100 nM TEA$_4$Thio-pRib-AMP (Thio-pRib-AMP) 1 d before *Pst* DC3000 spray inoculation. Bacteria colony forming units (CFU) were counted at 0 and 3 d post inoculation (0 and 3 dpi). Different shapes indicate independent experiments (n:3 or 6 biological replicates each for 0 and 3 dpi, respectively). Asterisks indicate statistically significant differences according to Student T-test. ***:*P*<0.0005; ns: non-significant, *P*>0.05. For box plots, the center line indicates the median, the bounds of the box show the 25th and the 75th percentiles, and the whiskers indicate 1.5 × IQR. **(f)** Disease symptoms of *B. napus* leaves derived from (e) at 3 dpi. Pictures are representative of n:6 leaves from three independent experiments. Scale bar: 1 cm.

Supplementary Files

This is a list of supplementary files associated with this preprint. Click to download.

- SupplementaryTable3Submission.xlsx
- SupplementaryinformationNatureBiotechSI.docx
- SupplementaryTable2Submission.xlsx
- SupplementaryTable1Submission.xlsx
- ExtendedDataFigures.docx